

Control of liquid crystal skyrmions towards designing re-configurable materials

Ayhan Duzgun, Avadh Saxena

*Theoretical Division and Center for Nonlinear Studies,
Los Alamos National Laboratory, Los Alamos, New Mexico 87545, USA*

Jonathan V. Selinger

Liquid Crystal Institute and Department of Physics, Kent State University Kent, OH, 44242, USA

Recently there has been significant research efforts towards materials by design, self-assembly at various length scales, and functional soft materials. Here, we propose that skyrmions in chiral nematic liquid crystals are suitable building blocks for the realization the above goals due to the possibility of individually controlling them. Skyrmions have attracted much and rapidly growing interest due to their topological properties and unique aspects for potential novel applications such as data storage and soft robotics. While not real particles, these skyrmions behave like particles they interact with each other and can be actuated by means of electric field, surface anchoring, and light. On the other hand, they are field configurations which have properties not possessed by real particles. In this letter, we outline some of the basic mechanisms and knobs by which LC skyrmions can be confined and moved for realization of custom material properties. Our work may trigger experimental efforts in this direction.

INTRODUCTION

In his famous 1959 speech on early ideas regarding nanotechnology Richard Feynman said [1], *I can hardly doubt that when we have some control of the arrangement of things on a small scale we will get an enormously greater range of possible properties that substances can have, and of different things that we can do.* In this paper, we propose that liquid crystal (LC) skyrmions can be used, along the line of such purposes, to realize *quasi-materials* with desired properties at the micro scale and outline the main components of design principles and driving mechanisms.

Skyrmions are particle-like topological field configurations which were originally proposed as field configurations in particle physics [2], and later their realization in magnetic systems attracted much attention and extensive research has uncovered many complex features of magnetic skyrmions [3]. More recently LC skyrmions, the subject of this work, have been realized as micron sized solitons in a chiral nematic material confined between two parallel substrates [4–8]. See Fig. 1 a,b.

In a LC system, some of the properties that make skyrmions favorable for individual design and manipulation are as follows. First of all they exist as isolated *local* objects [6] unlike other structures such as merons (half-skyrmions) that are generally reported to exist in lattices [9–13]. Second, they interact with other skyrmions as soft repulsive particles [14–16] (unless tilted). Furthermore, as also we show in this paper, they can be confined and moved. In addition to these particle-like properties, skyrmions are flexible and deformable, their interaction can be switched between isotropic-repulsive and directional-attractive [14], and they respond to external fields and light in interesting ways [17]. Skyrmions can be generated and decimated individually at will at

targeted locations in a desired fashion [6]. These features lacked by real particles provide an even richer set of tools for realizing *control of the arrangement of things*.

In this this work we focus on control knobs that will allow utilizing LC skyrmions for material realizations or functional emergent behaviors. First, we investigate the range of parameter space in which skyrmions can be realized and how that range can be escaped to decimate the skyrmions. Next, we introduce confinement and guidance of skyrmions by means of external fields, light exposure, and patterned director configurations on the confining surfaces, namely surface anchoring. Finally we demonstrate how these soft and hard wall mechanisms can be utilized to move skyrmions.

ISOLATED SKYRMIONS BETWEEN CHOLESTERIC AND UNIFORM NEMATIC PHASES: SIZE AND SHAPE

Consider a *LC cell* consisting of a chiral nematic LC confined between two parallel plates patterned with homeotropic surface anohring. In addition, an electric field perpendicular to the plates is applied. Let us chose the axis perpendicular to the surfaces to be z . Then the surface anchoring will enforce alignment of LC molecules along the z axis, so called *easy-axis* alignment, while the alignment due to the electric field can be either easy axis or *easy-plane*, perpendicular to z , depending on the dielectric properties of the confined LC.

We use Q-tensor representation to describe the average orientation of LC molecules at a certain position which is defined as $Q_{\alpha\beta} = \frac{3}{2} (\langle n_\alpha n_\beta \rangle - \frac{1}{3} \delta_{\alpha\beta})$. In this notation Landau-de Gennes type free energy per unit volume can

be expressed as

$$\begin{aligned}
F = & \frac{1}{2}a\text{Tr}(Q^2) + \frac{1}{3}b\text{Tr}(Q^3) + \frac{1}{4}c[\text{Tr}(Q^2)]^2 \\
& + \frac{1}{2}L(\partial_\gamma Q_{\alpha\beta})(\partial_\gamma Q_{\alpha\beta}) - 2q_0L\epsilon_{\alpha\beta\gamma}Q_{\alpha\rho}\partial_\gamma Q_{\beta\rho} \\
& - (\Delta\epsilon E^2 Q_{zz} - K[\delta(z) + \delta(z - N_z)])Q_{zz} \quad (1)
\end{aligned}$$

where the first line shows the thermal part with coefficients a , b , and c and the second line represents elastic terms with elastic constant L and natural twist q_0 .

Without the third line, the system exhibits cholesteric phase for low chirality and blue phases for high chirality. A very strong easy-axis alignment will unwind the cholesteric stripes and result in a vertical nematic phase. Between no alignment and strong alignment there exists a range for metastable isolated skyrmions[7, 8, 12, 18, 19].

Alignment is achieved by adding the third line which represents the effects of surface anchoring K , at $z = 0$ and $z = N_z$, and external electric field E , where $\Delta\epsilon$ is the difference of two dielectric constants along and perpendicular to the long axis of LC molecules. Positive value of $\Delta\epsilon$ indicates a material with easy-axis alignment while a negative value represents a material with easy-plane alignment.

Numerical solution to the above free energy equation is obtained by simulations with over-damped relaxation dynamics, which is detailed in the methods section.

In this section we explore the effect of electric field, surface anchoring and cell thickness on the size and shape of skyrmions.

First, we would like to explore how 3D director profiles of the skyrmions can be controlled by means of the two aligning forces used. In Fig. 1-b, director configurations of skyrmions for various K and α combinations are depicted. It is possible to sustain skyrmions by solely surface anchoring, solely electric field or a combination of both with dielectric anisotropy of either sign. For stronger K values skyrmions take a barrel shape (spherulite) whose top and bottom ends combine with defect loops or points. As K is reduced and α is increased, the defect loops disappear into the surfaces and form structures that we shall refer to as 2D skyrmions (despite a slight narrowing at the ends). In the limit of very small surface anchoring and practically the field alone, we have a z -invariant structure which in simulations can be modeled by a single layer in order to lower the computational cost.

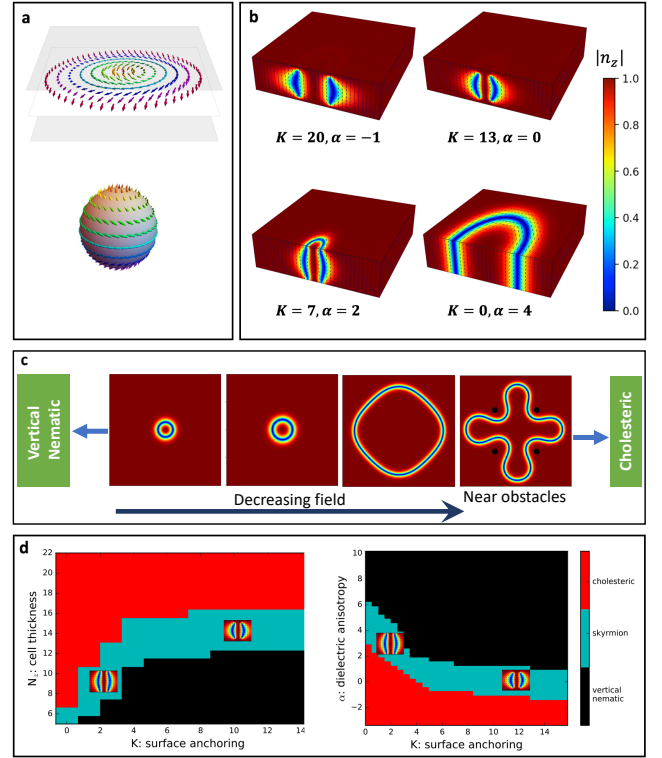


FIG. 1. Skyrmions realized in a chiral LC host confined between two parallel plates. (a) Director configuration on the midplane of a skyrmion and its mapping on to a sphere is shown. (b) Surface anchoring K and dielectric anisotropy α can be used in various combinations to realize 3D and 2D (z invariant) skyrmions. The unit of K is $K_0 = LSq_0$ and the unit of α is $\alpha_0 = LSq_0^2$. $N_z = 29$ and $p = 80$ (c) Top view of A 2D skyrmion is shown. As the background easy-axis alignment is varied, the skyrmions are metastable between vertical nematic and cholesteric phases. (d) Left: for no field ($\alpha = 0$) cell thickness vs. surface anchoring phase diagram of skyrmions. Right: for $N_z = 15$, field vs. surface anchoring phase diagram

Next, we would like to explore the limits of the alignment strength and the effects of it on the size of the skyrmions. Unlike real particles, skyrmion size is strongly coupled to the background field. For instance, in Fig. 1-c the size of a single layer skyrmion (in reality a very thin film) varies greatly with background field. As the field is increased the skyrmion shrinks and disappears. On the other hand, as the field is decreased, the skyrmion becomes much larger and more *flexible* and even deforms around obstacles (fixed vertical background) without breaking. For detailed analytical and numerical calculations we refer the reader to our previous work on 2D skyrmions [12]. The same behavior is observed for skyrmions in thicker cells, when both electric field and surface anchoring are present. The strength of surface anchoring K , cell thickness N_z , the electric field alignment α are the three factors that play a role. For clarity, we fix one of the three and vary the other two to illustrate

the range in which the skyrmions will exist. Fig. 1-d shows two different graphs regarding the parameter range for skyrmions between cholesteric and vertical nematic phases. For instance, left plot shows skyrmions realized using only surface anchoring. As the cell thickness N_z is reduced we generate a bigger effective easy-axis alignment. Thus, very thin cells yield a vertical nematic, thick cells yield a cholesteric phase and there is a range in between which allows skyrmions. For smaller K values, the skyrmions are free from defect loops (2D skyrmions). However for bigger K values, defect loops appear. On the right hand side, we keep the cell thickness fixed at $N_z = 15$ and vary α . Similarly the skyrmions exist between cholesteric and vertical nematic phases and are 2D for smaller K values and 3D for bigger K values.

WALLS MADE OF STRONG VERTICAL ALIGNMENT: SKYRMION-WALL AND SKYRMION-SKYRMION INTERACTION

The director profile of a skyrmion on a vertical cross section is basically a kink—the director points up in the left far field, down at the center of the skyrmion and then up again far right. For an isolated skyrmion embedded in a uniform far field, the 180° rotation from the center to the far right (or left) has a decay length that can be used to define a size for the skyrmion. That size, determined by the natural twist together with frustration in the system, is roughly a measure of how far away the skyrmion wants to be from the perfectly vertical far field. Therefore, if we enforce a vertical alignment in a region we will essentially generate a wall that will keep the skyrmions away. It is also intuitive that two skyrmions near one another will repel each other due to the same reason—relaxation of gradients.

Next, we would like to investigate the range of interaction between a skyrmion and a wall. To do this, we initially place a skyrmion near a wall and let the system relax until the skyrmion stops moving. Similarly for skyrmion-skyrmion interaction, we also place two skyrmions near one another and wait until they reach a separation at which movement stops. In Fig. 2 we plot skyrmion-skyrmion and skyrmion-wall equilibrium distances for 2D and 3D skyrmions of various sizes controlled by alignment strength. In the case of 2D skyrmions, we set $K = 0$ and vary α . For the 3D skyrmions, we set $\alpha = 0$ and vary K . R is the distance from the skyrmion center over which the 90° rotation occurs (radius of the blue circle) and x is the equilibrium distance from skyrmion center to the wall or midpoint between two skyrmions.

The results illustrate that the rotations are asymmetric around the horizontal director circle (blue circle). By varying the alignment strength (α or K) we generate significant change in R and x but their difference varies very

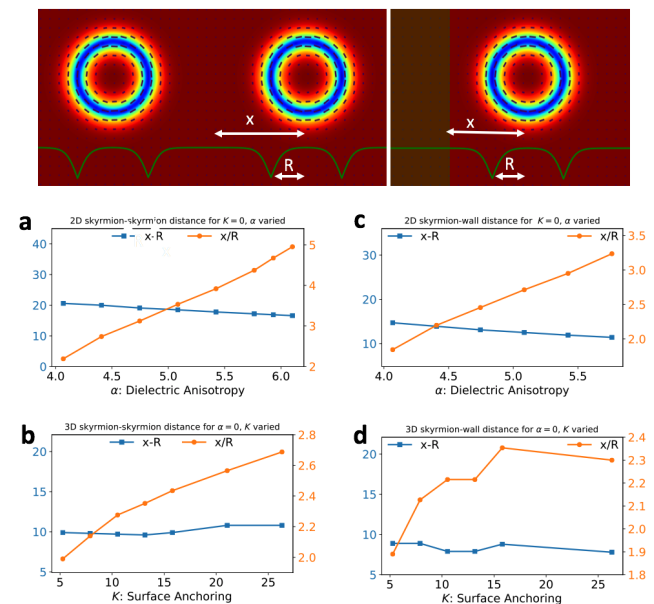


FIG. 2. Top: Two nearby skyrmions and a skyrmion near a wall (produced by a strong vertical alignment) are shown. Green lines indicate the absolute value of director n_z . R is skyrmion radius and x is distance from skyrmion center to the mid-point/wall. (a-d) Orange lines show x/R and solid blue lines show $x - R$. (a) 2D skyrmion-skyrmion distance. (b) 3D skyrmion-skyrmion distance. (c) 2D wall-skyrmion distance. (d) 3D wall-skyrmion distance.

slightly. This clearly shows that while rotation from 0° to 90° varies with alignment strength, rotation from 90° to 180° takes place over an almost constant distance. Our expectation was that both skyrmion size and range of interaction would be proportional to the cholesteric pitch. Contrary to this expectation, the range of interaction is not a certain multiple of R but varies and can reach multiple skyrmion sizes. The cholesteric pitch in these simulations is $p = 40$ lattice units thus for 2D skyrmions, surface to surface distance is $\approx p$ while wall to surface distance is $\approx \frac{3}{8}p$. For 3D skyrmions both distances are about $\approx \frac{1}{4}p$.

REPULSIVE OR ATTRACTIVE REGIONS

Confinement and controlled motion of skyrmions are essential features in order to custom design materials. Surface anchoring is one way to impose boundary conditions for this purpose. Similarly, field alignment can produce regions with desired director configuration. While surface anchoring requires pre-processing and is permanent, electric fields in principle can be turned on and off, moved, reoriented and varied with desired time dependence. Next, we would like to explore how regions with alignment that are stronger or weaker than the back-

ground interact with skyrmions.

The wall mechanism described in the previous section can be used to generate repulsive regions. By the same token regions with weaker alignment will act as attractive walls or regions. One can think in terms of energies as well. As mentioned above, the director profile of a skyrmion cross section can be viewed as a vertical inner disk surrounded by a π wall and then the director relaxes to being vertical over some distance. Energetically the gradients of Q must be minimized. Therefore, an external field which enforces vertical alignment will favor an overlap with vertical parts of the skyrmion resulting in repelling the skyrmion's horizontal parts (blue circle). Similarly if a skyrmion is near a locally lower alignment region, the horizontal (or *less vertical*) directors would prefer to overlap with that region resulting in attraction.

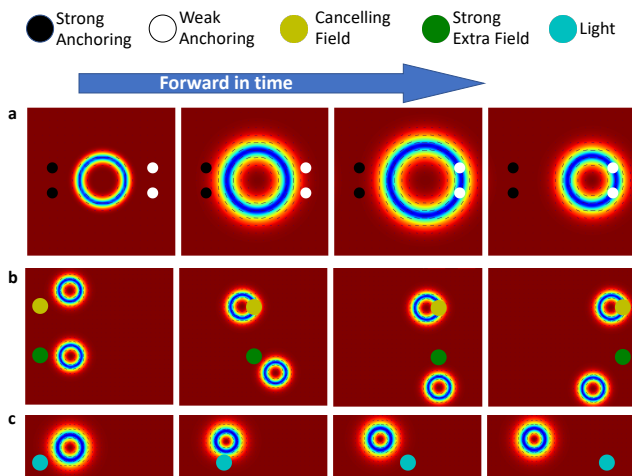


FIG. 3. Snapshots from simulations showing skyrmions near moving or stationary spots made by modifications in surface anchoring, field, or light. (a) A skyrmion is swollen by lowering the background field so it comes in contact with nearby spots. It is then repelled by strong anchoring sites (black) and attaches to the weak anchoring sites (white). (b) Skyrmions are dragged by low field spot (yellow) and repelled by high field spot (green). (c) Skyrmions are repelled by moving light.

Simulation snapshots in Fig. 3 are some arrangements which generate repulsive or attractive regions. In (a), surface anchoring is patterned. Black circles mark regions with strong anchoring and white circles mark regions with weak surface anchoring. Initially the skyrmion is placed in between and then the background field is reduced so that the skyrmion swells and interacts with the black and white regions. Finally, the field is brought to the initial value to deswell the skyrmion. In the final picture, the skyrmion ends up adhering to the weaker anchoring sites. In part (b), green spots denote regions with stronger electric field in the z direction and yellow spots denote the regions in which the background field is canceled by electric field applied in the opposite direction.

Once these spots are moved towards the skyrmions, the stronger field repels and the weak field attracts, therefore drags them. In part (c), we show snapshots demonstrating a different mechanism, light exposure. Exposure to light chemically increases the helical pitch of some LC materials [20, 21]. To model the effect of light in simulations, we reduce the natural twist q_0 by a factor, here 1.5, in the region of exposure. When we move that region towards a skyrmion, the skyrmion is repelled away from light. Our simulations confirm that reduction in q_0 is a valid mechanism to generate repulsive sites realized in experiments. All of these mechanisms can be used alone or in combination to generate patterned repulsive and/or attractive regions. (See supplementary material for movies of each of the above mechanisms).

Can skyrmions be combined when squeezed together? As a test, we placed skyrmions between moving walls and reduced the volume between the walls (supplementary material). As the walls move closer like a *trash compactor* no skyrmions fused. Interestingly, as the *pressure* increases the skyrmions get smaller and smaller until they pop spontaneously.

Non-uniform extra field

In the demonstrations above, we employed a uniform extra field produced in an area as small fraction of a skyrmion and this may seem difficult to achieve experimentally. In principle, the cross section of the field does not have to be small compared to skyrmion size to push or drag skyrmions. Also, the cholesteric pitch of the chiral LC can be tens of microns making it easier to stabilize bigger skyrmions. Furthermore, skyrmions in small background fields and weak surface anchoring conditions can allow skyrmion sizes larger than the cholesteric pitch. However, in other cases fringe effects caused by the small size of the electrodes will be important. Here we would like to address the case of very small electrodes placed on both sides of the LC cell.

When a potential difference ΔV is applied between two such electrodes, charges of opposite sign and equal magnitude of $q = C\Delta V$ will accumulate at the electrodes where C is the capacitance. For very small size limit, we can safely assume that they are point charges. In Fig. 4 we show how a field generated by two oppositely charged point sources can drive skyrmions. (Videos of simulations and the details of the discussion on how we model the effect of small electrodes are shown in the supplementary material). In part (a) of the figure, a relatively weaker field is applied. In part (b), even when the extra field is much bigger than the background field leading to obvious deviation of the directors from the vertical direction, skyrmions are still driven in the same fashion as in the presence of a uniform field. The main difference from the case a uniform field is that the vertical component

of the field will smoothly drop along the skyrmion radius, thus the field region will have some effective radius determined by the strength of the potential difference applied between the electrodes. Comparison of (a) and (b) panels of Fig. 4 illustrates how this size depends on the potential difference applied across. This feature adds another useful *knob* to the tool set to control skyrmions because changing the size of a repulsive (attractive) pillar by means of varying the potential difference is so much easier than changing electrode properties.

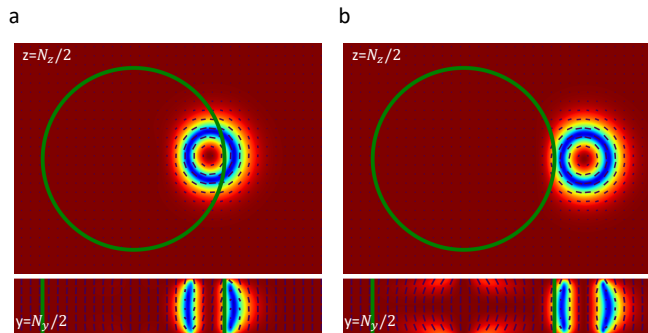


FIG. 4. **Repulsive site generated by a non-uniform extra field:** Skyrmions driven by moving extra field (inside green circle). $N_z/p = 16/40$, $K/LSq_0 = 7.9$ and $\alpha/LSq_0^2 = 1.7$ with material parameters listed in SM. Top panel shows horizontal cross section at $z = N_z/2$ and bottom panel shows vertical cross section at $y = N_y/2$. Point charges are placed at a distance $N_z/2 \pm 15$ above and below the mid-plane of the LC cell. The potential difference (charge) is chosen such that the ratio of the extra field at the midpoint of the cell to the background field is equal to (a) 1 and (b) 6. Comparison of (a) and (b) panels illustrates that a greater potential difference generates a greater effective size of the repulsive region.

DISCUSSION

We have outlined how electric field, surface anchoring and light can be useful control knobs in order to design systems of liquid crystal skyrmions. In addition to upright skyrmions, tilted skyrmions achieved by means of modulated or tilted background fields offer even richer features and interesting skyrmion behaviors in the presence of field, light, and surface anchoring are continuously being discovered. In this paper, we suffice by demonstrating basic tools one can utilize for custom designing material properties and leave the exciting physical properties mentioned above for future work. The methods presented here can easily be modified or expanded to realize many diverse features for applications. The possibilities are numerous, and the ground is open for realiza-

tions of innovative ideas. As first steps, we have already realized (numerically) some useful and physics-rich applications including skyrmionic artificial spin ice [22], and dynamic switching of skyrmion lattice structures on substrates [23]. Original experimental studies that appear recently also indicate that we are at the verge of significant progress in realizing functional materials whose constituents are skyrmions. Mechanisms in this work are based on important physical principals. We believe that the ideas presented here will motivate experimental and theoretical efforts to investigate the underlying physics in more detail. Furthermore, due to similarities between magnetic and LC skyrmions, similar methods and mechanisms can potentially help with progress in magnetic skyrmion research as well.

METHODS

Simulations were carried out using our home developed C++/CUDA code which allows parallel computation on the latest Nvidia Tesla-V100 graphics cards located at LANL. Free energy expressed in Eq. 1 was minimized using the overdamped dynamic equation,

$$\frac{\partial Q_{\alpha\beta}(\mathbf{r}, t)}{\partial t} = -\Gamma \frac{\delta F}{\delta Q_{\alpha\beta}(\mathbf{r}, t)} \quad (2)$$

where Γ is a mobility constant. Five independent components of the 3D Q -tensor defined on a cubic lattice were updated according to

$$Q_{\alpha\beta}(t + \Delta t) = Q_{\alpha\beta}(t) + \frac{\partial Q_{\alpha\beta}}{\partial t} \Delta t \quad (3)$$

where $\partial Q/\partial t$ is obtained from Eqn. 2 using finite differences method to calculate the derivatives. The numerical values for coefficients are $a = -40$, $b = -60$, $c = 100$, $q_0 = \pi(p = 40 \text{ lattice units})$, $L = 0.01$, $\Gamma\Delta t = 0.001$. The corresponding reduced chirality is $\kappa = \sqrt{108cLq_0^2/b^2} = 0.5$. The observed scalar order parameter after relaxation $S \approx 0.6$. An exception to these parameters skyrmions in Fig. 1-b. There we used $a = -100$, $b = -100$, and $p = 80$ lattice units.

By dividing the free energy density equation (Eq. 1), we see that the unit of energy density, surface anchoring K , and field alignment strength (α) is Lq_0^2 , LSq_0 , and LSq_0^2 respectively. For typical values of $p = 2 \mu\text{m}$ and $L = 10 \text{ pN}$, the thermal parameters can be calculated the following way. $a = (-40) \times \frac{(Lq_0^2)_{\text{real}}}{(Lq_0^2)_{\text{simulation}}} = (-40) \times \frac{10 \text{ pN}}{0.01} \times \left(\frac{\pi/\mu\text{m}}{\pi}\right)^2 = -0.4 \times 10^5 \text{ J/m}^3$. Similarly $b = -0.6 \times 10^5 \text{ J/m}^3$ and $c = 10^5 \text{ J/m}^3$.

This work was supported in part by the U.S. Department of Energy.

Supplementary Material

ELECTRIC FIELD INSIDE DIELECTRIC SLAB PLACED BETWEEN POINT ELECTRODES

A mechanism to generate walls that repel *upright* skyrmions stabilized in a chiral nematic liquid crystal (LC) cell is to produce extra vertical alignment by means of strong additional field. Here we explore how this can be done when the field cross section is very small and its magnitude and direction are not uniform.

We investigate the alignment effect of applying a potential difference between two very thin electrodes placed on both sides of liquid crystal cell. The LC cell itself is filled with a chiral nematic material with positive dielectric anisotropy that hosts full skyrmions. This requires, apart from the potential we will apply, already existing vertical alignment produced by homeotropic surface anchoring or a background electric field perpendicular to the plane of the cell because skyrmions are embedded in a uniform vertical far-field director. To generate a hard wall (a region with strong vertical alignment) the field from the applied potential should be much bigger than these existing alignment factors.

We will assume that the tips of the electrodes are very small spheres thus the charge accumulated at the tips will be modeled as point charges of equal magnitude but apposite sign symmetrically placed around the LC cell (Fig. 1).

First let's consider only the potential from one electrode perform the calculation with very slight modification of the method introduced by [24].

POTENTIAL INSIDE DIELECTRIC SLAB NEAR A POINT CHARGE

A point charge q is placed near a dielectric slab with dielectric constant ϵ . If the dielectric medium was semi-infinite as in [25], rather than a slab, the potential inside the dielectric medium would be equivalent to the potential due to the original charge plus one image charge overlapping with the original charge with magnitude $q' = -\beta q$ where $\beta = (\epsilon - \epsilon_0)/(\epsilon + \epsilon_0)$. However for the slab, another image charge is needed in order to satisfy the boundary conditions on the second plane. In turn additional charges will be required because boundary conditions on the first plane won't be satisfied anymore. Then the additional charges will require more image charges and so on.

Therefore it is seen that the infinite set of image charges shown in Fig. 5 is one way to get the solution for the potential at a point between the planes. The first image charge overlaps with the original charge. Thus to calculate the second image charge we can use the total charge $q - \beta q = (1 - \beta)q$ as *felt* at the location of the charge that is . At each step, the next image is found by locating it symmetrically about the plane of the corresponding surface charges and multiplying the magnitude of the charge by β . At a point on the axis of symmetry located at distances x_1 from the surface closer to the charge q and x_2 from the surface away from q , the potential due to the charges on the right side is

$$V_R = \frac{(1 - \beta)q}{4\pi\epsilon_0(x_1 + h)} + \frac{(1 - \beta)q\beta^2}{4\pi\epsilon_0(x_1 + h + 2d)} + \dots = \frac{(1 - \beta)q}{4\pi\epsilon_0} \sum_{n=0}^{\infty} \frac{\beta^{2n}}{x_1 + h + 2nd}.$$

Similarly, for the charges on the left hand side

$$V_L = \frac{(1 - \beta)q\beta}{4\pi\epsilon_0(x_2 + h + d)} + \frac{(1 - \beta)q\beta^3}{4\pi\epsilon_0(x_2 + h + 3d)} + \dots = \frac{(1 - \beta)q}{4\pi\epsilon_0} \sum_{n=0}^{\infty} \frac{\beta^{2n+1}}{x_2 + h + (2n + 1)d}.$$

The potential due to all charges are then

$$V = \frac{(1 - \beta)q}{4\pi\epsilon_0} \sum_{n=0}^{\infty} \left(\frac{\beta^{2n}}{x_1 + h + 2nd} + \frac{\beta^{2n+1}}{x_2 + h + (2n + 1)d} \right) \quad (4)$$

At a radial distance r from the central axis of the slab (line connecting the charges) is

$$V = \frac{(1 - \beta)q}{4\pi\epsilon_0} \sum_{n=0}^{\infty} \left(\frac{\beta^{2n}}{\sqrt{r^2 + (x_1 + h + 2nd)^2}} + \frac{\beta^{2n+1}}{\sqrt{r^2 + (x_2 + h + (2n + 1)d)^2}} \right) \quad (5)$$

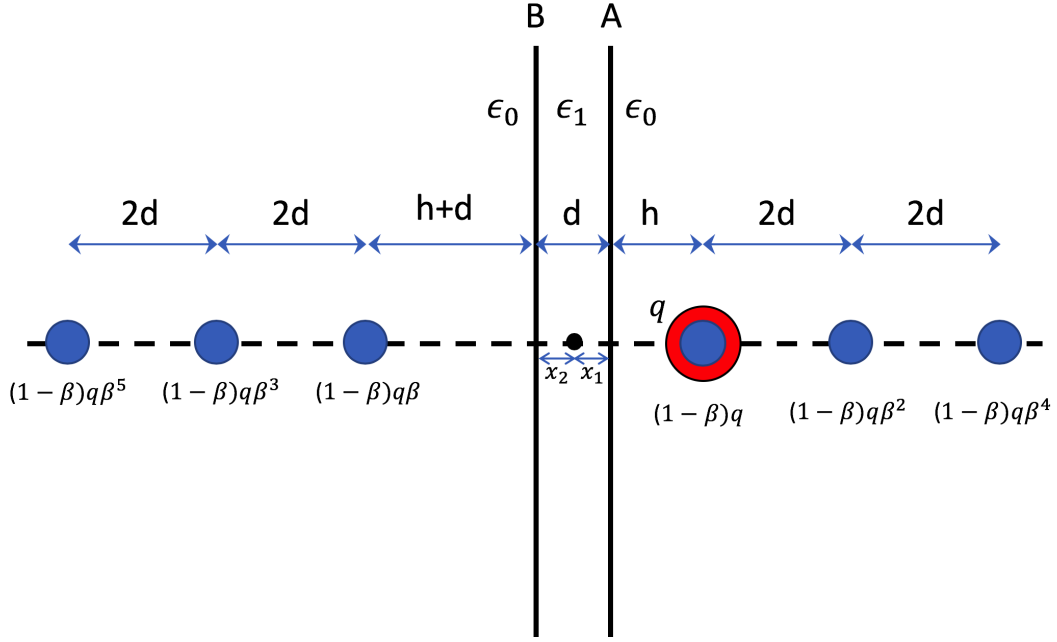


FIG. 5. **Calculation of the potential inside a slab by the method of image charges:** Red circle represents the original free charge q placed at a distance h from the right side of the slab of thickness d . Blue circles denote the infinite series of image charges at the positions shown. $\beta = (\epsilon - \epsilon_0)/(\epsilon + \epsilon_0)$.

POTENTIAL FROM TWO POINT CHARGES LOCATED ON SIDES OF A LC CELL

Using the result of the single charge case, potential inside the dielectric slab from two oppositely charged electrodes can be written, after swapping x_1 and x_2 for $-q$, as

$$V = \frac{(1-\beta)q}{4\pi\epsilon_0} \sum_{n=0}^{\infty} \left(\frac{\beta^{2n}}{\sqrt{r^2 + (x_1 + h + 2nd)^2}} + \frac{\beta^{2n+1}}{\sqrt{r^2 + (x_2 + h + (2n+1)d)^2}} - \frac{\beta^{2n}}{\sqrt{r^2 + (x_2 + h + 2nd)^2}} - \frac{\beta^{2n+1}}{\sqrt{r^2 + (x_1 + h + (2n+1)d)^2}} \right) \quad (6)$$

which then can be simplified by combining the terms with denominators containing x_1 or x_2 :

$$V = \frac{(1-\beta)q}{4\pi\epsilon_0} \sum_{n=0}^{\infty} \left(\frac{(-\beta)^n}{\sqrt{r^2 + (x_1 + h + nd)^2}} - \frac{(-\beta)^n}{\sqrt{r^2 + (x_2 + h + nd)^2}} \right) \quad (7)$$

where x_1 is the distance to the plane closer to $+q$ and x_2 is the distance to the plane closer to $-q$.

LC CELL BETWEEN ELECTRODES

A similar result to the above solution is obtained by [26] for a different arrangement of LC cell and coating. We argue(expect?) that typical arrangements of LC material, glass substrates, coatings etc. will yield similar potentials as long as the system consists of planar surfaces. Therefore as a generic example we use the dielectric slab described above.

We position the slab of thickness d at the origin. Two point charges $\pm q$ are placed at $z = \mp H$ respectively. Distances from the point where the field calculated are $x_1 + h = H - z$ and $x_2 + h = H + z$. Then $E_z = -\partial_z V$ and $E_r = -\partial_r V$ reads

$$E_z = \frac{(1-\beta)q}{4\pi\epsilon_0} \sum_{n=0}^{\infty} \left(\frac{(-\beta)^n(nd + H - z)}{[(nd + H - z)^2 + r^2]^{3/2}} + \frac{(-\beta)^n(nd + H + z)}{[(nd + H + z)^2 + r^2]^{3/2}} \right) \quad (8)$$

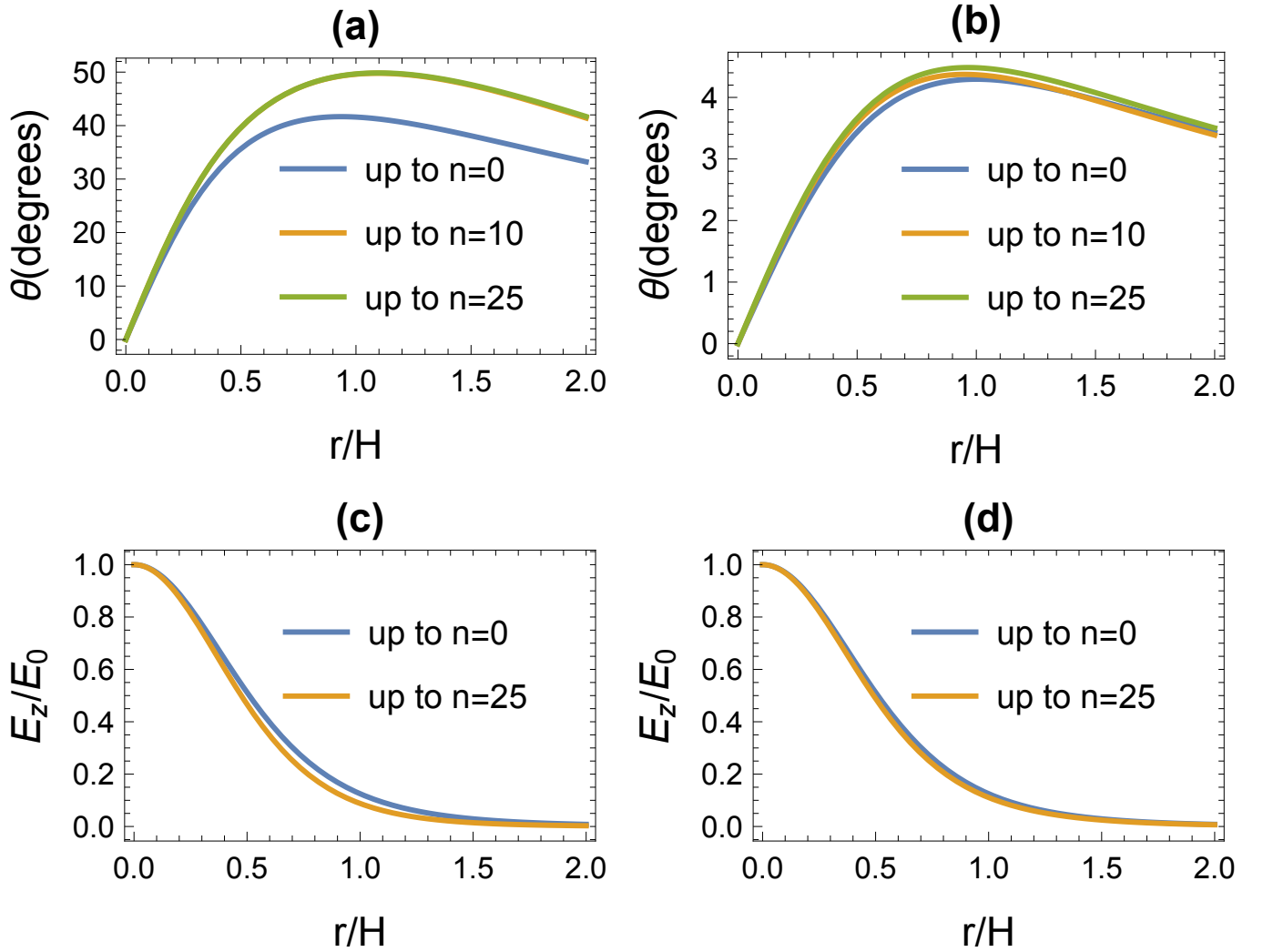


FIG. 6. **Comparison of fields calculated from Eqs. 8 and 9 using first n terms.** Top: Angle of electric field measured from z -axis for (a) $d = H$. (b) $d = 0.1H$. Bottom: $E_z(z = 0)$ normalized by $E_0 = E_z(z = 0, r = 0)$ up to indicated number of terms for (c) $d = H$. (d) $d = 0.1H$.

$$E_r = \frac{(1 - \beta)q}{4\pi\epsilon_0} \sum_{n=0}^{\infty} \left(-\frac{(-\beta)^n r}{[(nd + H - z)^2 + r^2]^{3/2}} + \frac{(-\beta)^n r}{[(nd + H + z)^2 + r^2]^{3/2}} \right) \quad (9)$$

Next we compare the full sum of series to only the first term substituting dielectric coefficient $\epsilon = 10$ (anisotropy ignored for simplicity) and $\beta = (10 - 1)/(10 + 1) \approx 0.8$. In Fig. 6 we plot E_z and the deviation of field lines from the vertical direction i.e $\theta = \arctan(E_r/E_z)$ as a function of r/H for two different values of the cell thickness d .

Conclusion

Regardless of how many terms we use to calculate the fields a more important feature is that E_z decays to zero within a radius $r \leq 2H$. This enables to create pillars made of electric field with size less than $2H$. The actual effective radius will depend on various parameters and it can be directly controlled by varying the potential difference across the electrodes which enables us to achieve pillar sizes that can be varied from very small to big values.

As for how much approximation is appropriate, Fig 6 illustrates that, the first terms in Eq. 9 and 8 capture the essential features of the exact sum. In the simulations, since we normalize the extra field by the value at the origin (middle of the dielectric slab), the first term E_z is very close to the infinite sum (Fig. 6-(c),(d)). Therefore we can

say that fields from two point charges will be sufficient to capture the physics, although there is not much difficulty in including more terms for numerical calculations.

-
- [1] R. Feynman, *Caltech Engineering and Science* **23:5**, 22 (1960).
 - [2] T. Skyrme, *Nuclear Physics* **31**, 556 (1962).
 - [3] S. Mühlbauer, B. Binz, F. Jonietz, C. Pfleiderer, A. Rosch, A. Neubauer, R. Georgii, and P. Böni, *Science* **323**, 915 (2009).
 - [4] J.-i. Fukuda and S. Zumer, *Nature Communications* **2**, 246 EP (2011), article.
 - [5] A. N. Bogdanov, U. K. Röbber, and A. A. Shestakov, *Phys. Rev. E* **67**, 016602 (2003).
 - [6] P. J. Ackerman, R. P. Trivedi, B. Senyuk, J. van de Lagemaat, and I. I. Smalyukh, *Phys. Rev. E* **90**, 012505 (2014).
 - [7] S. Afghah and J. V. Selinger, *Phys. Rev. E* **96**, 012708 (2017).
 - [8] Y. Guo, S. Afghah, J. Xiang, O. D. Lavrentovich, R. L. B. Selinger, and Q.-H. Wei, *Soft Matter* **12**, 6312 (2016).
 - [9] R. M. Hornreich and S. Shtrikman, *Phys. Rev. A* **41**, 1978 (1990).
 - [10] A. Nych, J.-i. Fukuda, U. Ognysta, S. Zumer, and I. Musevic, *Nature Physics* **13**, 1215 EP (2017), article.
 - [11] L. Metselaar, A. Doostmohammadi, and J. M. Yeomans, *The Journal of Chemical Physics* **150**, 064909 (2019), <https://doi.org/10.1063/1.5085282>.
 - [12] A. Duzgun, J. V. Selinger, and A. Saxena, *Phys. Rev. E* **97**, 062706 (2018).
 - [13] S. Wang, M. Ravnik, and S. Umer, *Liquid Crystals* **45**, 2329 (2018), <https://doi.org/10.1080/02678292.2018.1512168>.
 - [14] P. J. Ackerman, J. van de Lagemaat, and I. I. Smalyukh, *Nature Communications* **6**, 6012 EP (2015), article.
 - [15] D. Foster, C. Kind, P. J. Ackerman, J.-S. B. Tai, M. R. Dennis, and I. I. Smalyukh, *Nature Physics* (2019), 10.1038/s41567-019-0476-x.
 - [16] N. Nagaosa and Y. Tokura, *Nature Nanotechnology* **8**, 899 EP (2013), review Article.
 - [17] H. Sohn, P. Ackerman, and I. Smalyukh, in *APS Meeting Abstracts* (2017) p. A17.013.
 - [18] I. I. Smalyukh, B. I. Senyuk, P. Palfy-Muhoray, O. D. Lavrentovich, H. Huang, E. C. Gartland, V. H. Bodnar, T. Kosa, and B. Taheri, *Phys. Rev. E* **72**, 061707 (2005).
 - [19] G. Durey, H. R. O. Sohn, P. J. Ackerman, E. Brasselet, I. I. Smalyukh, and T. Lopez-Leon, *Soft Matter*, (2020).
 - [20] H. R. O. Sohn, P. J. Ackerman, T. J. Boyle, G. H. Sheetah, B. Fornberg, and I. I. Smalyukh, *Phys. Rev. E* **97**, 052701 (2018).
 - [21] H. R. O. Sohn, C. D. Liu, Y. Wang, and I. I. Smalyukh, *Opt. Express* **27**, 29055 (2019).
 - [22] A. Duzgun and C. Nisoli, “Artificial spin ice of liquid crystal skyrmions,” (2019), arXiv:1908.03246 [cond-mat.soft].
 - [23] A. Duzgun, C. Nisoli, C. J. O. Reichhardt, and C. Reichhardt, “Commensurate states and pattern switching via liquid crystal skyrmions trapped in a square lattice,” (2019), arXiv:1911.10270 [cond-mat.soft].
 - [24] S. Tometani, *Eur. J. Phys.* **21**, 549554 (2000).
 - [25] J. J. D., ‘*Classical Electrodynamics*’ (New York: Wiley, 1975) p. 1479.
 - [26] R. J. M. Fushan Zhou, DengKe Yang, *Journal of Information Display* **3:4**, 8 (2002).